



CrossMark  
click for updates

Cite this: *RSC Adv.*, 2015, 5, 85460

# Branched and linear A<sub>2</sub>–D–A<sub>1</sub>–D–A<sub>2</sub> isoindigo-based solution-processable small molecules for organic field-effect transistors and solar cells†

Mirco Tomassetti,<sup>abc</sup> Farid Ouhib,<sup>a</sup> Ilaria Cardinaletti,<sup>c</sup> Pieter Verstappen,<sup>b</sup> Alberto Salleo,<sup>d</sup> Christine Jérôme,<sup>a</sup> Jean Manca,<sup>e</sup> Wouter Maes<sup>\*bf</sup> and Christophe Detrembleur<sup>\*a</sup>

To establish a correlation between the molecular structure, physicochemical properties, thin film morphology, charge carrier mobility and photovoltaic performance of isoindigo-based electron donor type molecular semiconductors, a series of branched and linear A<sub>2</sub>–D–A<sub>1</sub>–D–A<sub>2</sub> small molecules (A = acceptor, D = donor) are synthesized. The extended  $\pi$ -conjugated molecular chromophores have an electron-accepting isoindigo core, a bridging oligothiophene electron donor part and terminal octyl cyanoacrylate acceptor moieties. Their photophysical, thermal and electrochemical properties are analysed and the materials are applied in organic field-effect transistors and bulk heterojunction organic solar cells. Compared to an analogous benzothiadiazole-based small molecule, the isoindigo core deepens the HOMO energy level, enabling higher open-circuit voltages in organic solar cells. The linear isoindigo-based small molecule shows an enhanced hole mobility compared to the branched derivatives. The best power conversion efficiency of the investigated set is also obtained for the solar cell based on the linear (CA-3T-IID-3T-CA-I) donor molecule in combination with PC<sub>71</sub>BM.

Received 31st August 2015  
Accepted 1st October 2015

DOI: 10.1039/c5ra17660c

[www.rsc.org/advances](http://www.rsc.org/advances)

## 1. Introduction

Conjugated organic small molecules and oligomers have received quite some attention for applications in organic electronics because of their solution processability and potential toward fabrication of light-weight and flexible large area electronic devices.<sup>1–4</sup> In recent years, solution-processed small molecule organic field-effect transistors (OFETs) with charge carrier mobilities above 10 cm<sup>2</sup> V<sup>–1</sup> s<sup>–1</sup> have been reported.<sup>5–7</sup> On the other hand, bulk heterojunction (BHJ) small molecule organic solar cells with power conversion efficiencies (PCEs) in the range of 5–10% have been developed.<sup>8–14</sup> Compared to their conjugated polymer counterparts, ‘small’ molecules have

noticeable advantages regarding synthetic simplicity and purification, well defined chemical and electronic structure, and reproducible properties, which allows to establish relationships between molecular and optoelectronic device parameters in a more straightforward manner.<sup>15,16</sup> Such deepened fundamental insights are essential for further development of the OFET and OPV (organic photovoltaics) fields and projected market entrance.

Various donor–acceptor type small molecules based on a multitude of electron-deficient groups (*e.g.* squaraine,<sup>17</sup> benzotriazole,<sup>18</sup> alkyl cyanoacetate,<sup>19</sup> diketopyrrolopyrrole,<sup>20</sup> benzothiadiazole,<sup>21</sup> and isoindigo<sup>22</sup>), most often combined with electron-donating oligothiophenes or arylamine units, have been developed over the years. The donor–acceptor (D–A) structure allows to lower the HOMO–LUMO gap and thereby to increase the absorption width. Among the electron-poor components, isoindigo (IID) is a promising molecular building block for solar cell and transistor applications because of its straightforward large-scale synthesis, strong light absorption, photochemical stability and stacking tendency.<sup>22–27</sup> It has been coupled with a variety of electron-rich groups to provide numerous low band gap polymers and related small molecules for BHJ OPV devices.<sup>24,26,28–36</sup>

In recent years, it has been shown that the architecture of small molecule semiconductors is a crucial parameter that strongly influences the electronic properties of the materials and the final device outcome.<sup>37–43</sup> Further clarification of the

<sup>a</sup>Center for Education and, Research on Macromolecules (CERM), University of Liège (Ulg), Chemistry Department, Sart-Tilman B6A, 40009 Liège, Belgium. E-mail: christophe.detrembleur@ulg.ac.be

<sup>b</sup>Design & Synthesis of Organic Semiconductors (DSOS), Institute for Materials Research (IMO-IMOME), Hasselt University, Agoralaan 1 – Building D, 3590 Diepenbeek, Belgium. E-mail: wouter.maes@uhasselt.be

<sup>c</sup>Material Physics Division, Hasselt University, Universitaire Campus – Wetenschapspark 1, 3590 Diepenbeek, Belgium

<sup>d</sup>Department of Materials Science and Engineering, Stanford, California 94305, USA

<sup>e</sup>X-Lab, Hasselt University, Agoralaan 1 – Building D, 3590 Diepenbeek, Belgium

<sup>f</sup>IMEC, IMOME, Universitaire Campus – Wetenschapspark 1, 3590 Diepenbeek, Belgium

† Electronic supplementary information (ESI) available. See DOI: 10.1039/c5ra17660c

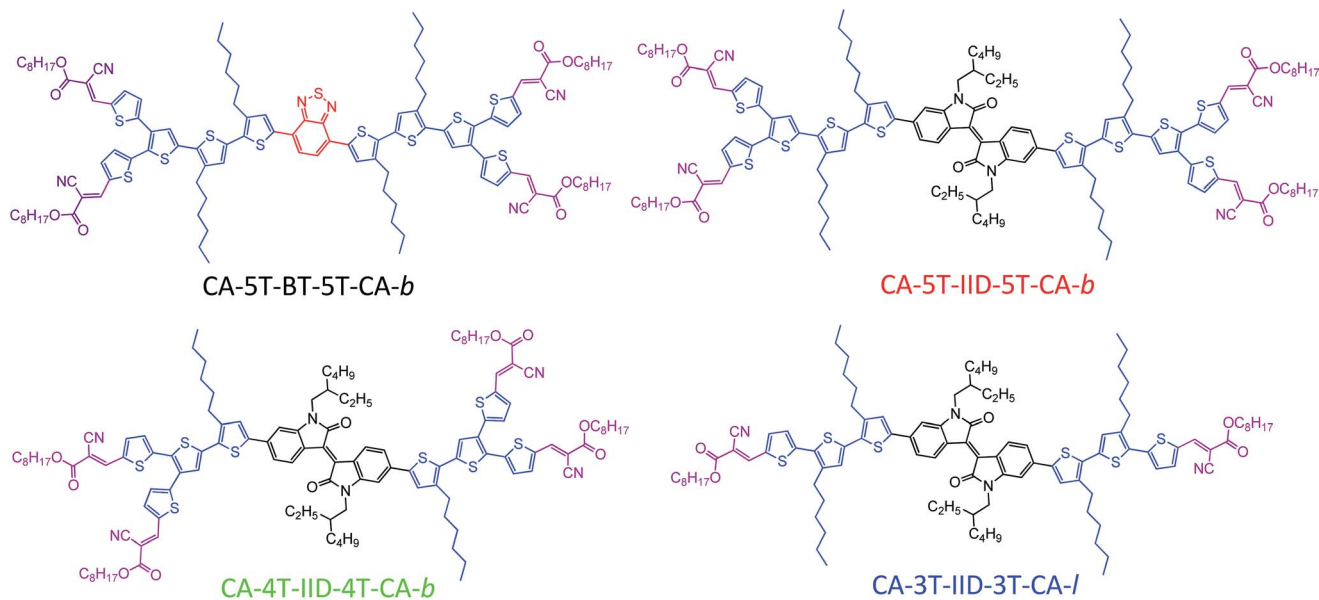


Fig. 1 Chemical structures of the small molecule semiconductors CA-5T-BT-5T-CA-b, CA-5T-IID-5T-CA-b, CA-4T-IID-4T-CA-b and CA-3T-IID-3T-CA-l.

molecular architecture–(device) property relationships is required, though, to fully exploit the synthetic versatility toward top-efficiency devices. In this work, we describe the synthesis and characterization of one linear (l) and three branched (b) A<sub>2</sub>–D–A<sub>1</sub>–D–A<sub>2</sub> type small molecules (Fig. 1). The central unit of these materials is either a benzothiadiazole (BT) or an isoindigo molecule and a number of (alkyl)thiophene units (xT), increasing solubility and conjugation length, link these cores to (a different number of) cyanoacrylate (CA) electron-deficient end groups.<sup>19,44–48</sup> The final materials are analysed in OFET and BHJ OPV devices.

## 2. Experimental

### 2.1. Materials

N-2-Ethylhexyl-substituted 6,6'-dibromoisindigo (**1**),<sup>36</sup> (3-hexylthiophene-5-yl)trimethylstannane (**2**)<sup>49</sup> and {5,5''-bis(5,5-dimethyl-1,3-dioxan-2-yl)-[2,2':3',2''-terthiophen]-5'-yl}trimethylstannane (**7**)<sup>50</sup> were prepared according to literature methods. Small molecules CA-5T-BT-5T-CA-b and CA-4T-IID-4T-CA-b were previously developed as photoinitiators (in combination with an iodonium salt) for the cationic polymerization of vinyl ethers.<sup>50</sup> All other chemicals were obtained from Aldrich and used as received. Solvents were distilled over standard drying agents under dry nitrogen.

### 2.2. Instruments and measurements

NMR spectra were recorded on Bruker AVANCE 250 or 400 MHz spectrometers. MALDI-TOF mass spectra were recorded on a Bruker Daltonics Ultraflex II Tof/Tof. 1 μL of the matrix solution (16 mg mL<sup>-1</sup> DTCB (*trans*-2-[3-(4-*tert*-butylphenyl)-2-methyl-2-propenylidene]malononitrile) in CHCl<sub>3</sub>) was spotted onto an MTP Anchorchip 600/384 MALDI plate. The spot was

allowed to dry and 1 μL of the analyte solution (0.5 mg mL<sup>-1</sup> in CHCl<sub>3</sub>) was spotted on top of the matrix. Reported masses are for the first isotope peak of the isotopic pattern. Optical absorption spectra were taken on a Cary 500 scan UV-vis spectrometer. Electrochemical measurements were performed with an Eco Chemie Autolab PGSTAT 30 potentiostat/galvanostat using a three-electrode microcell with a platinum wire working electrode, a platinum wire counter electrode and an anhydrous Ag/AgNO<sub>3</sub> reference electrode (Ag/0.1 M NBU<sub>4</sub>PF<sub>6</sub> in MeCN containing 0.01 M AgNO<sub>3</sub>). The small molecules were deposited onto the working electrode from chloroform solutions. The samples were analyzed in anhydrous acetonitrile containing 0.1 M NBU<sub>4</sub>PF<sub>6</sub>. The electrolyte solution was degassed with Ar prior to each measurement. To prevent air from entering the system, a curtain of Ar was maintained during the experiments. Cyclic voltammograms were recorded at a scan rate of 100 mV s<sup>-1</sup>. The HOMO and LUMO frontier energy levels were calculated from the equation  $E_{(HOMO/LUMO)}$  (eV) =  $-1 \times (E_{ox/red}^{onset} \text{ vs. Ag/AgNO}_3 - E_{Fc/Fc^+}^{onset} \text{ vs. Ag/AgNO}_3) - 4.98$ . The onset potentials were referenced to ferrocene/ferrocenium, which has an ionization potential of  $-4.98$  eV vs. vacuum. This correction factor is based on a value of 0.31 eV for Fc/Fc<sup>+</sup> vs. SCE<sup>51</sup> and a value of 4.68 eV for SCE vs. vacuum.<sup>52</sup> Differential scanning calorimetry (DSC) measurements were acquired on a TA Instruments Q1000 DSC using standard aluminium pans, an indium standard for calibration, and nitrogen as the purge gas. Melting and crystallization temperatures were determined by taking the peak values of the second heating and cooling scans. The nanomorphologies of the pure small molecule and blend films were acquired in PeakForce Tapping™ mode with a Bruker Multimode 8 AFM, with Scan Asyst™ enabled. The silicon nitride cantilevers had a nominal spring constant of 4 N m<sup>-1</sup>. Scans were performed in air, and images were analysed

and corrected for aberration through the use of the free Gwyddion software.

### 2.3. Synthesis

**Compound 3.** *N*-2-Ethylhexyl-substituted 6,6'-dibromoisindigo **1** (550 mg, 0.85 mmol, 1 equiv.) and (3-hexylthiophene-5-yl)trimethylstannane (**2**) (622 mg, 1.88 mmol, 2.2 equiv.) were placed in a dry round-bottom flask (50 mL) with Pd<sub>2</sub>(dba)<sub>3</sub> (31 mg, 0.03 mmol, 4 mol%) and P(*o*-tol)<sub>3</sub> (26 mg, 0.08 mmol, 10 mol%). The flask was evacuated and backfilled with Ar three times. Next, anhydrous toluene (20 mL) was added through a septum and the mixture was stirred for 24 h at 100 °C under Ar. After removal of the solvent under reduced pressure, the crude material was purified by silica gel chromatography, eluting with CH<sub>2</sub>Cl<sub>2</sub>-hexanes (1-3), to yield a purple solid (574 mg, 82%). <sup>1</sup>H NMR (CDCl<sub>3</sub>, 250 MHz): δ (ppm) 9.14 (d, <sup>3</sup>J<sup>H-H</sup> = 7.5 Hz, 2H), 7.30-7.23 (m, 6H), 6.95 (s, 2H), 3.78-3.61 (m, 4H), 2.64 (t, <sup>3</sup>J<sup>H-H</sup> = 7.5 Hz, 4H), 1.93-1.81 (m, 2H), 1.71-1.61 (m, 4H), 1.44-1.27 (m, 28H), 0.99-0.87 (m, 18H).

**Compound 4.** *N*-Bromosuccinimide (NBS) (270 mg, 1.52 mmol, 2.2 equiv.) was added at 0 °C to a solution of compound **3** (566 mg, 0.69 mmol, 1 equiv.) in THF (15 mL). After stirring for 12 h, an aqueous solution of sodium bicarbonate was added and the product was extracted with dichloromethane. The organic phase was washed with water, dried with MgSO<sub>4</sub>, filtered and concentrated under reduced pressure. The residue was purified by silica gel chromatography, eluting with CH<sub>2</sub>Cl<sub>2</sub>-hexanes (1-3), to yield a dark solid (573 mg, 85%). <sup>1</sup>H NMR (CDCl<sub>3</sub>, 250 MHz): δ (ppm) 9.14 (d, <sup>3</sup>J<sup>H-H</sup> = 7.5 Hz, 2H), 7.19 (d, <sup>3</sup>J<sup>H-H</sup> = 7.5 Hz, 2H), 7.09 (s, 2H), 6.86 (d, <sup>4</sup>J<sup>H-H</sup> = 2.5 Hz, 2H), 3.74-3.67 (m, 4H), 2.59 (t, <sup>3</sup>J<sup>H-H</sup> = 7.5 Hz, 4H), 1.90-1.82 (m, 2H), 1.68-1.57 (m, 4H), 1.43-1.27 (m, 28H), 0.99-0.89 (m, 18H).

**Compound 5.** Compound **4** (520 mg, 0.53 mmol, 1 equiv.) and (3-hexylthiophene-5-yl)trimethylstannane (**2**) (388 mg, 1.17 mmol, 2.2 equiv.) were placed in a dry round-bottom flask (50 mL) with Pd<sub>2</sub>(dba)<sub>3</sub> (19 mg, 0.02 mmol, 4 mol%) and P(*o*-tol)<sub>3</sub> (16 mg, 0.05 mmol, 10 mol%). The flask was evacuated and backfilled with Ar three times. Next, anhydrous toluene (10 mL) was added through a septum and the mixture was stirred for 24 h at 100 °C under Ar. After removal of the solvent under reduced pressure, the crude material was purified by silica gel chromatography, eluting with CH<sub>2</sub>Cl<sub>2</sub>-hexanes (1-3), to yield a pure blue solid (589 mg, 96%). <sup>1</sup>H NMR (CDCl<sub>3</sub>, 250 MHz): δ (ppm) 9.14 (d, <sup>3</sup>J<sup>H-H</sup> = 7.5 Hz, 2H), 7.25-7.23 (m, 4H), 7.02 (s, 2H), 6.94-6.92 (m, 4H), 3.75-3.67 (m, 4H), 2.78 (t, <sup>3</sup>J<sup>H-H</sup> = 7.5 Hz, 4H), 2.63 (t, <sup>3</sup>J<sup>H-H</sup> = 7.5 Hz, 4H), 1.91-1.85 (m, 2H), 1.74-1.60 (m, 8H), 1.44-1.29 (m, 40H), 0.99-0.88 (m, 24H).

**Compound 6.** NBS (175 mg, 0.98 mmol, 2.2 equiv.) was added at 0 °C to a solution of compound **5** (515 mg, 0.44 mmol, 1 equiv.) in THF (20 mL). After stirring for 12 h, an aqueous solution of sodium bicarbonate was added and the product was extracted with dichloromethane. The organic phase was washed with water, dried with MgSO<sub>4</sub>, filtered and concentrated under reduced pressure. The residue was purified by silica gel chromatography, eluting with CH<sub>2</sub>Cl<sub>2</sub>-hexanes (1-3), to yield a dark

blue solid (561 mg, 96%). <sup>1</sup>H NMR (CDCl<sub>3</sub>, 250 MHz): δ (ppm) 9.14 (d, <sup>3</sup>J<sup>H-H</sup> = 7.5 Hz, 2H), 7.24 (d, <sup>3</sup>J<sup>H-H</sup> = 7.5 Hz, 2H), 7.22 (s, 2H), 6.93 (s, 2H), 6.87 (s, 2H), 3.75-3.67 (m, 4H), 2.74 (t, <sup>3</sup>J<sup>H-H</sup> = 7.5 Hz, 4H), 2.58 (t, <sup>3</sup>J<sup>H-H</sup> = 7.5 Hz, 4H), 1.90-1.83 (m, 2H), 1.70-1.59 (m, 8H), 1.43-1.25 (m, 40H), 0.99-0.87 (m, 24H).

**Compound 9.** Compound **6** (430 mg, 0.33 mmol, 1 equiv.) and compound **7** (503 mg, 0.79 mmol, 2.4 equiv.) were placed in a dry round-bottom flask (50 mL) with Pd<sub>2</sub>(dba)<sub>3</sub> (12 mg, 0.01 mmol, 4 mol%) and P(*o*-tol)<sub>3</sub> (10 mg, 0.03 mmol, 10 mol%). The flask was evacuated and backfilled with Ar three times. Next, anhydrous toluene (10 mL) was added through a septum and the mixture was stirred for 24 h at 100 °C under Ar. After removal of the solvent under reduced pressure, the crude material was purified by silica gel chromatography, eluting with THF-hexanes (1-9), to yield a pure blue solid (510 mg, 74%). <sup>1</sup>H NMR (CDCl<sub>3</sub>, 250 MHz): δ (ppm) 9.15 (d, <sup>3</sup>J<sup>H-H</sup> = 7.5 Hz, 2H), 7.63-7.60 (m, 2H), 7.43-7.40 (m, 2H), 7.17 (s, 2H), 7.03-6.95 (m, 12H), 5.62 (s, 4H), 3.78-3.60 (m, 20H), 2.85-2.75 (m, 8H), 1.93-1.83 (m, 2H), 1.75-1.65 (m, 8H), 1.48-1.25 (m, 64H), 0.97-0.85 (m, 24H).

**Compound 10.** Compound **6** (124 mg, 0.09 mmol, 1 equiv.) and [5-(5,5-dimethyl-1,3-dioxan-2-yl)thiophen-2-yl]trimethylstannane (**8**) (82 mg, 0.23 mmol, 2.4 equiv.) were placed in a dry round-bottom flask (50 mL) with Pd<sub>2</sub>(dba)<sub>3</sub> (4 mg, 0.003 mmol, 4 mol%) and P(*o*-tol)<sub>3</sub> (3 mg, 0.01 mmol, 10 mol%). The flask was evacuated and backfilled with Ar three times. Next, anhydrous toluene (10 mL) was added through a septum and the mixture was stirred for 24 h at 100 °C under Ar. After removal of the solvent under reduced pressure, the crude material was purified by silica gel chromatography, eluting with THF-hexanes (1-9), to yield a pure blue solid (132 mg, 90%). <sup>1</sup>H NMR (CDCl<sub>3</sub>, 250 MHz): δ (ppm) 9.13 (d, <sup>3</sup>J<sup>H-H</sup> = 7.5 Hz, 2H), 7.25-7.23 (m, 4H), 7.11-7.10 (m, 2H), 7.03-7.00 (m, 4H), 6.92 (s, 2H), 5.65 (s, 2H), 3.81-3.64 (m, 12H), 2.83-2.73 (m, 8H), 1.93-1.82 (m, 2H), 1.76-1.62 (m, 8H), 1.43-1.28 (m, 52H), 0.99-0.86 (m, 24H).

**CA-5T-IID-5T-CA-b.** Pyridinium *p*-toluene sulfonate (239 mg, 0.95 mmol, 4 equiv.) was dissolved in a minimum volume of an acetone-water (4-1) mixture and added to a solution of compound **9** (500 mg, 0.24 mmol, 1 equiv.) in THF (20 mL). After stirring the mixture for 24 h at 90 °C, the reaction was quenched with water and the product was extracted with dichloromethane. The organic phase was washed with brine, dried with MgSO<sub>4</sub>, filtered and concentrated under reduced pressure. The obtained crude product (300 mg, 0.17 mmol, 1 equiv.) was dissolved in 10 mL of chloroform. Two droplets of triethylamine and octylcyanoacetate (336 mg, 1.71 mmol, 10 equiv.) were added. After stirring for 24 h at ambient temperature, the solvent was evacuated under reduced pressure and the dark product was purified by silica gel chromatography, eluting with CHCl<sub>3</sub>-hexanes (1-1), to yield a pure green solid (317 mg, 54% over both steps). <sup>1</sup>H NMR (CDCl<sub>3</sub>, 400 MHz): δ (ppm) 9.14 (d, <sup>3</sup>J<sup>H-H</sup> = 7.5 Hz, 2H), 8.32 (s, 2H), 8.24 (s, 2H), 7.78 (d, <sup>3</sup>J<sup>H-H</sup> = 2.5 Hz, 2H), 7.74 (d, <sup>3</sup>J<sup>H-H</sup> = 2.5 Hz, 2H), 7.28-7.24 (m, 12H), 7.08 (s, 2H), 6.96 (s, 2H), 4.34-4.29 (m, 8H), 3.81-3.74 (m, 4H), 2.85 (t, <sup>3</sup>J<sup>H-H</sup> = 7.5 Hz, 8H), 1.93-1.86 (m, 2H), 1.80-1.71 (m, 16H), 1.45-0.91 (m, 80H), 1.01-0.90 (m, 36H). <sup>13</sup>C

(APT) NMR (CDCl<sub>3</sub>, 100 MHz):  $\delta$  (ppm) 168.7, 162.7, 146.2, 145.8, 145.7, 143.7, 141.8, 141.7, 141.4, 137.8, 137.7, 137.5, 137.2, 136.6, 135.4, 132.2, 131.8, 131.5, 131.2, 128.9, 128.7, 128.5, 128.1, 127.4, 121.2, 115.8, 104.6, 99.4, 99.3, 66.7, 37.8, 31.8, 31.7, 30.9, 30.5, 29.7, 29.6, 29.3, 29.22, 29.18, 29.15, 29.0, 28.5, 25.8, 24.4, 23.1, 22.6, 14.2, 14.14, 14.11, 10.9. MALDI-TOF MS: calcd for C<sub>144</sub>H<sub>178</sub>N<sub>6</sub>O<sub>10</sub>S<sub>10</sub>2471.1; found  $m/z$  2471.5 [M]<sup>+</sup>, 2494.5 [M + Na]<sup>+</sup>.

**CA-3T-IID-3T-CA-I.** Pyridinium *p*-toluene sulfonate (40 mg, 0.16 mmol, 2 equiv.) was dissolved in a minimum volume of an acetone–water (4–1) mixture and it was added to a solution of compound **10** (123 mg, 0.079 mmol, 1 equiv.) in THF (20 mL). After stirring the mixture for 24 h at 90 °C, the reaction was quenched with water and the product was extracted with dichloromethane. The obtained crude product (100 mg, 0.073 mmol, 1 equiv.) was dissolved in 5 mL of chloroform. One droplet of triethylamine and octylcyanoacetate (72 mg, 0.36 mmol, 5 equiv.) were added. After stirring for 24 h at ambient temperature, the solvent was evacuated under reduced pressure and the dark product was purified by silica gel chromatography, eluting with CHCl<sub>3</sub>–hexanes (1–1), to yield a blue solid (81 mg, 59% over both steps). <sup>1</sup>H NMR (CDCl<sub>3</sub>, 400 MHz):  $\delta$  (ppm) 9.16 (d, <sup>3</sup>*J*<sup>H–H</sup> = 8 Hz, 2H), 8.27 (s, 2H), 7.78 (d, <sup>3</sup>*J*<sup>H–H</sup> = 4 Hz, 2H), 7.27–7.25 (m, 6H), 7.07 (s, 2H), 6.93 (s, 2H), 4.32 (t, <sup>3</sup>*J*<sup>H–H</sup> = 8 Hz, 4H), 3.81–3.66 (m, 4H), 2.89–2.81 (m, 8H), 1.92–1.87 (m, 2H), 1.81–1.70 (m, 12H), 1.45–1.32 (m, 60H), 1.01–0.90 (m, 30H). <sup>13</sup>C (APT) NMR (CDCl<sub>3</sub>, 100 MHz):  $\delta$  (ppm) 168.6, 163.1, 146.4, 145.8, 145.6, 143.0, 142.0, 141.7, 138.0, 137.7, 136.5, 134.8, 131.8, 131.0, 129.5, 129.3, 127.5, 126.1, 118.8, 116.1, 104.6, 97.7, 66.6, 37.8, 31.8, 31.7, 30.9, 30.4, 30.3, 30.0, 29.8, 29.31, 29.27, 29.20, 29.18, 29.0, 28.6, 25.8, 24.4, 23.2, 22.66, 22.62, 14.2, 14.1, 10.9. MALDI-TOF MS: calcd for C<sub>104</sub>H<sub>136</sub>N<sub>4</sub>O<sub>6</sub>S<sub>6</sub>1728.9; found  $m/z$  1729.0 [M]<sup>+</sup>, 1752.1 [M + Na]<sup>+</sup>.

#### 2.4. Fabrication and characterization of the organic solar cells

The (standard architecture) photovoltaic devices were fabricated using pre-patterned ITO-coated glass substrates. They were cleaned with detergent, followed by ultrasonication in water, acetone, and isopropyl alcohol. After complete drying, the substrates were treated with UV/ozone for 15 min. As a buffer layer, PEDOT:PSS (CLEVIOS P VP.Al 4083) was spin-coated on top of the ITO-coated glass substrates, followed by annealing at 120 °C for 15 min to remove any residual water. The substrates were then transferred into a glove box filled with N<sub>2</sub>, where the active layers were spin-coated from chloroform solutions, aiming at thicknesses of ~100 nm (determined using a Dektak<sup>ST3</sup> surface profiler). The active layer solutions consisted of any of the four small molecules and PC<sub>71</sub>BM (Solenne) in different ratios and concentrations. To completely dissolve the molecules, the solutions were stirred overnight at 50 °C. Solvent-annealing was performed by exposing the active layers to a vapour of dichloromethane directly after deposition. Finally, the cathode double-layer was deposited by thermal evaporation of Ca (30 nm) and Al (80 nm). Devices with 3 mm<sup>2</sup> area were obtained. PCE's were calculated from the *J*–*V*

characteristics recorded on a Keithley 2400 under AM1.5 conditions, supplied by a Newport class A solar simulator (model 91195A). External quantum efficiencies (EQEs) were acquired by recording the monochromated (Newport Cornerstone 130 with sorting filters) output of a xenon lamp (100 W, Newport 6257) by a lock-in amplifier (Stanford Research Systems SR830). The light beam was mechanically chopped at 10 Hz. The recorded values were calibrated with a FDS-100 calibrated silicon photodiode.

#### 2.5. Fabrication and characterization of the OFETs

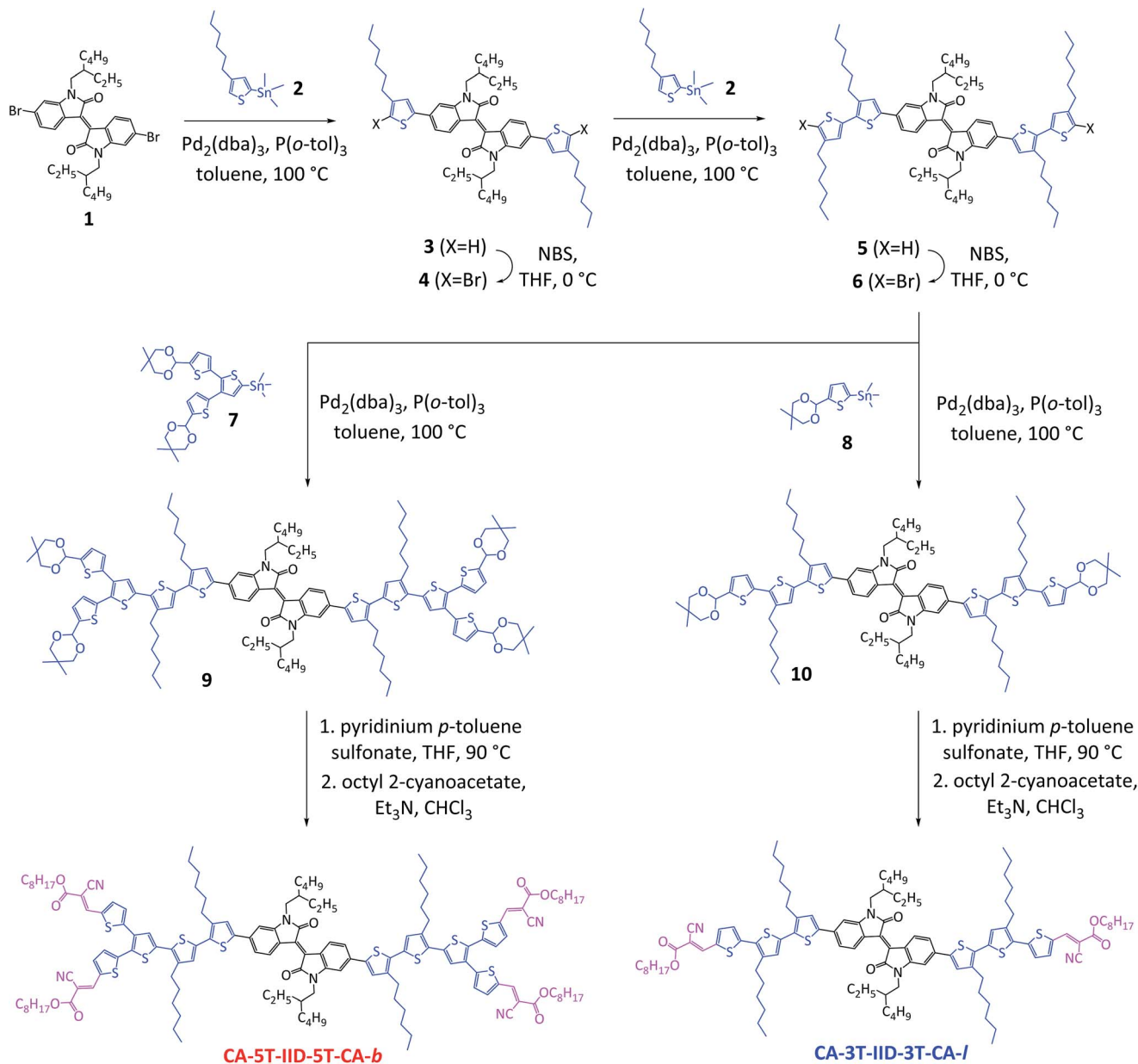
The hole mobilities of the small molecules were obtained from bottom-gate bottom-contacts OFET devices. The pure molecules were spin-coated from chloroform solutions on *n*-Si/SiO<sub>2</sub> substrates with pre-patterned, interdigitated titanium/gold source and drain contacts. The mobility ( $\mu$ ) was extracted operating in the saturated regime using devices with a channel length of 10  $\mu$ m. Solvent annealing was performed in the same way as described above for the solar cells.

### 3. Results and discussion

#### 3.1. Synthesis and characterization

The applied synthetic strategy towards the branched **CA-5T-IID-5T-CA-b** and linear **CA-3T-IID-3T-CA-I** small molecules is outlined in Scheme 1. The two other molecular semiconductors compared in the present study (**CA-5T-BT-5T-CA-b** and **CA-4T-IID-4T-CA-b**, Fig. 1) were made in an analogous fashion and were previously applied as photoinitiators (in combination with an iodonium salt) for the cationic polymerization of vinyl-ethers.<sup>50</sup> The initial IID precursor, *N*-2-ethylhexyl-substituted 6,6'-dibromoisindigo **1**, was synthesized by condensation of two commercially available compounds, 6-bromoisatin and 6-bromooxindole, in acetic acid and subsequent alkylation with 1-bromo-2-ethylhexane in the presence of K<sub>2</sub>CO<sub>3</sub> (94% yield).<sup>22</sup> This compound then underwent a Stille cross-coupling with (3-hexylthiophene-5-yl)trimethylstannane (**2**), using Pd<sub>2</sub>(dba)<sub>3</sub>/P(*o*-tol)<sub>3</sub> as the catalyst system (82% yield). Afterwards, bromination with *N*-bromosuccinimide (NBS) yielded the brominated derivative **4** (85% yield). This sequence – Stille cross-coupling with **2** and bromination – was then repeated to extend the molecule with two additional thiophene units (96% yield for both individual steps). Brominated precursor molecule **6** was then coupled by a Stille reaction with acetals **7** and **8** (protecting the aldehyde moieties required for the final condensation step) to afford branched derivative **9** (74% yield) and the linear analogue **10** (90% yield), respectively. After deprotection with the aid of pyridinium *p*-toluene sulfonate in THF, both compounds were reacted with octyl 2-cyanoacetate to give the branched (**CA-5T-IID-5T-CA-b**; 54% yield) and linear (**CA-3T-IID-3T-CA-I**; 59% yield) cyanoacrylate-terminated small molecules. The final products were carefully purified by silica gel chromatography and fully characterized.

UV-vis absorption spectra of the four small molecules in diluted chloroform solutions and thin films are shown in Fig. 2. The corresponding data are summarized in Table 1. The



Scheme 1 Applied synthetic routes towards small molecules CA-5T-IID-5T-CA-b and CA-3T-IID-3T-CA-I.

solution absorption spectra of the three IID derivatives are broader and red-shifted compared to the BT-based small molecule due to the stronger intramolecular donor–acceptor interaction. Indeed, CA-5T-BT-5T-CA-b shows two absorption bands covering the wavelength range from 350 up to 650 nm, with a maximum absorption at 382 nm, whereas the IID-based small molecules show extended absorption to over 700 nm. The IID materials have three absorption maxima at around 370, 480 and 590 nm. The branched derivatives show a maximum absorption in the UV region, whereas the linear molecule CA-3T-IID-3T-CA-I has a maximum absorption at 485 nm. The thin film absorption spectra of all four small molecules are broadened and exhibit red-shifted absorption maxima above 600 nm (Table 1), which can be attributed to increased intermolecular interactions and backbone planarity in the solid state.<sup>53</sup> Upon

(dichloromethane) solvent vapour annealing (SVA) of the films, minor additional red shifts can be seen (Fig. 2, Table 1). Based on the thin film absorption onsets, optical HOMO–LUMO gaps around 1.6 eV were obtained (Table 1).

Cyclic voltammetry (CV) was performed to investigate the electrochemical properties of the four small molecules and to get a first estimate of their HOMO–LUMO energy levels. The corresponding voltammograms are presented in Fig. 3 (Fig. S13<sup>†</sup>) and the data are gathered in Table 1. The HOMO and LUMO energy levels were derived from the onset potentials of the oxidation and reduction waves, respectively, using the onset potential of the Fc/Fc<sup>+</sup> redox couple as a reference. Due to the stronger electron acceptor properties of IID compared to BT, the IID-based small molecules exhibit (slightly) lower LUMO energy levels (mainly governed by the

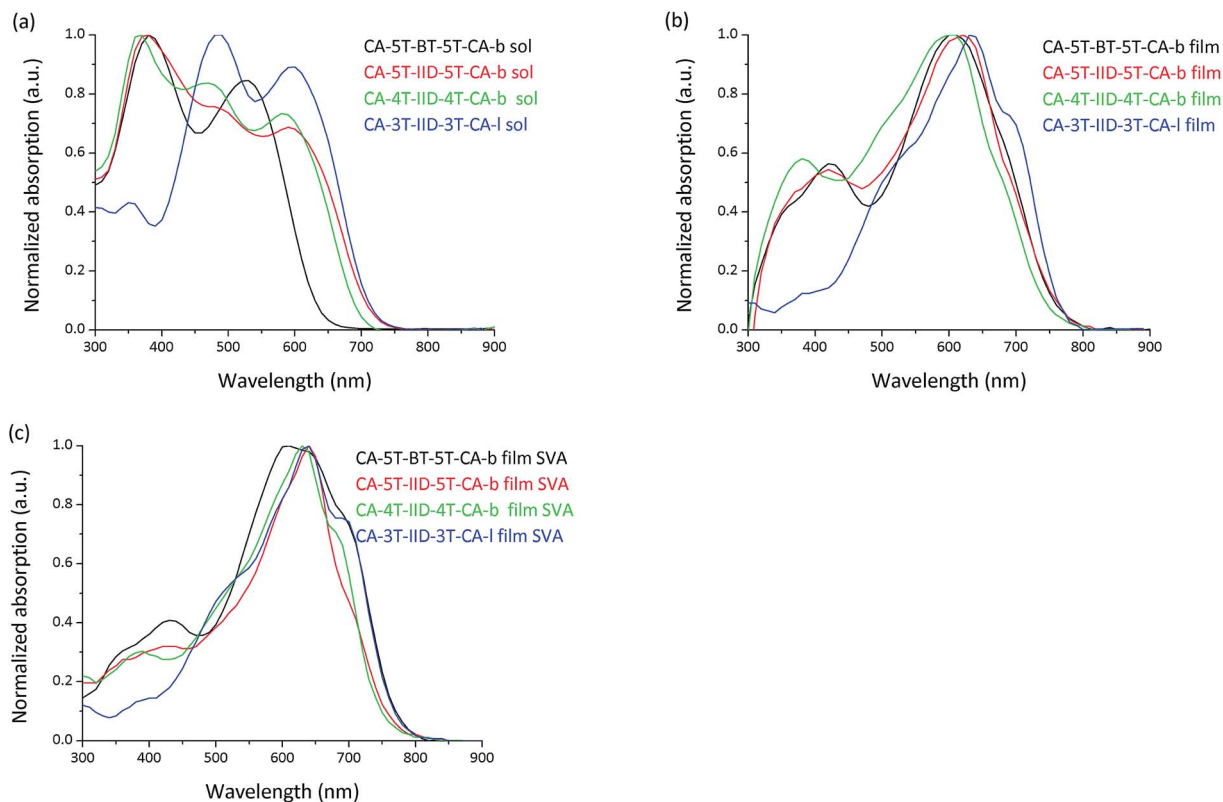


Fig. 2 Normalized UV-vis absorption spectra of small molecules CA-5T-BT-5T-CA-b (black), CA-5T-IID-5T-CA-b (red), CA-4T-IID-4T-CA-b (green), and CA-3T-IID-3T-CA-I (blue) in  $\text{CHCl}_3$  solution (a) and thin film before (b) and after (c) SVA.

Table 1 Overview of the optical and electrochemical properties of the small molecules

Small molecule	$\lambda_{\text{max}}^{\text{sol}}$ (nm)	$\epsilon^a$ ( $\text{M}^{-1} \text{cm}^{-1}$ )	$\lambda_{\text{max}}^{\text{film}}$ (nm)	$\lambda_{\text{max}}^{\text{film SVA}}$ (nm)	$E_{\text{g}}^{\text{opt}b}$ (eV)	$E_{\text{onset}}^{\text{ox}}$ (V)	$E_{\text{HOMO}}^c$ (eV)	$E_{\text{onset}}^{\text{red}}$ (V)	$E_{\text{LUMO}}^c$ (eV)	$E_{\text{g}}^{\text{ec}d}$ (eV)
CA-5T-BT-5T-CA-b	382	$8.87 \times 10^4$	606	616	1.58	0.24	-5.20	-1.42	-3.54	1.66
CA-5T-IID-5T-CA-b	375	$7.38 \times 10^4$	618	644	1.58	0.37	-5.33	-1.34	-3.62	1.71
CA-4T-IID-4T-CA-b	366	$6.86 \times 10^4$	602	634	1.62	0.56	-5.52	-1.36	-3.61	1.91
CA-3T-IID-3T-CA-I	485	$5.00 \times 10^4$	633	633	1.55	0.60	-5.56	-1.37	-3.59	1.97

<sup>a</sup> Extinction coefficients in  $\text{CHCl}_3$  solution. <sup>b</sup> Optical HOMO-LUMO gap taken from the absorption edge of the thin film UV-vis spectrum. <sup>c</sup> HOMO and LUMO values were calculated from the onset of oxidation and reduction, respectively. <sup>d</sup> Electrochemical HOMO-LUMO gap.

electron-deficient units<sup>54,55</sup>). On the other hand, the HOMO energy levels (mainly related to the electron donor part<sup>55</sup>) gradually go down upon decreasing the number of bridging thiophene units.<sup>56</sup>

The thermal properties of the molecular semiconductors were investigated by DSC (under  $\text{N}_2$  atmosphere at a scanning rate of  $10^\circ \text{C min}^{-1}$  in the range of  $40\text{--}250^\circ \text{C}$ ). As presented in Fig. 4 (Fig. S14<sup>†</sup>), all the materials show clear phase transitions. CA-5T-BT-5T-CA-b shows a melting trajectory with a maximum at  $200^\circ \text{C}$  ( $\Delta H_{\text{m}} = 34.6 \text{ J g}^{-1}$ ) and a crystallization peak with a maximum at  $161^\circ \text{C}$  ( $\Delta H_{\text{c}} = 32.7 \text{ J g}^{-1}$ ). On the other hand, two melting trajectories appear for the analogous branched IID-based small molecule CA-5T-IID-5T-CA-b, peaking at  $159^\circ \text{C}$  ( $\Delta H_{\text{m}} = 9.6 \text{ J g}^{-1}$ ) and  $219^\circ \text{C}$  ( $\Delta H_{\text{m}} = 16.0 \text{ J g}^{-1}$ ), pointing to two different polymorphs. Likewise, two crystallizations are

observed at  $189^\circ \text{C}$  ( $\Delta H_{\text{c}} = 17.9 \text{ J g}^{-1}$ ) and  $136^\circ \text{C}$  ( $\Delta H_{\text{c}} = 9.8 \text{ J g}^{-1}$ ). Removing one of the bridging thiophene units seems to increase the crystallinity, leading to a broad melting peak at a higher temperature of  $234^\circ \text{C}$  ( $\Delta H_{\text{m}} = 32.3 \text{ J g}^{-1}$ ) and a crystallization peak at  $220^\circ \text{C}$  ( $\Delta H_{\text{c}} = 30.3 \text{ J g}^{-1}$ ) for CA-4T-IID-4T-CA-b. For the linear CA-3T-IID-3T-CA-I small molecule, one very broad melting trajectory is observed between  $177$  and  $210^\circ \text{C}$  ( $\Delta H_{\text{m}} = 21.4 \text{ J g}^{-1}$ ) and one broad crystallization peak is seen at  $182^\circ \text{C}$  ( $\Delta H_{\text{c}} = 18.7 \text{ J g}^{-1}$ ).

### 3.2. OFETs

The hole mobilities of the four small molecules were measured by fitting OFET transfer characteristics (Table 2, Fig. S15–S18<sup>†</sup>). Films of pure CA-5T-BT-5T-CA-b show a hole mobility of  $1.44 \times 10^{-5} \text{ cm}^2 \text{ V}^{-1} \text{ s}^{-1}$ , significantly higher than observed for the

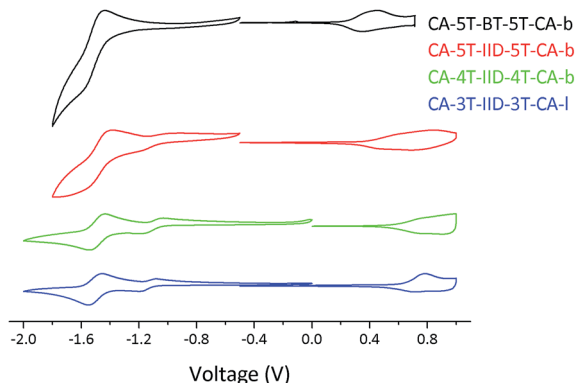


Fig. 3 Cyclic voltammograms obtained for drop-casted films of CA-5T-BT-5T-CA-b (black), CA-5T-IID-5T-CA-b (red), CA-4T-IID-4T-CA-b (green), and CA-3T-IID-3T-CA-I (blue) prepared from chloroform solutions.

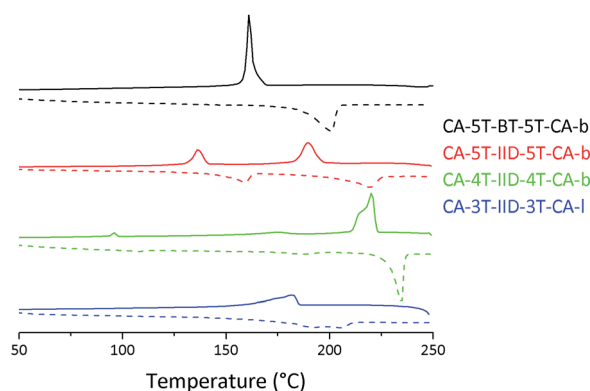


Fig. 4 DSC heating (dashed lines) and cooling (solid lines) scans for the small molecule materials (2<sup>nd</sup> heating and cooling, scan rate 10 °C min<sup>-1</sup>, exo up).

analogous IID-based material **CA-5T-IID-5T-CA-b** ( $3.75 \times 10^{-6} \text{ cm}^2 \text{ V}^{-1} \text{ s}^{-1}$ ). The removal of one hexylthiophene unit in the branched IID molecule (**CA-4T-IID-4T-CA-b**) does not affect the mobility to a large extent ( $4.26 \times 10^{-6} \text{ cm}^2 \text{ V}^{-1} \text{ s}^{-1}$ ). On the other hand, the linear **CA-3T-IID-3T-CA-I** molecule afforded a hole mobility of  $4.20 \times 10^{-4} \text{ cm}^2 \text{ V}^{-1} \text{ s}^{-1}$ , two orders of magnitude higher than the other IID-based materials. When

analysing the surface of the pure **CA-5T-BT-5T-CA-b** film (Fig. 5a), we noticed large crystallites, around 350 nm long and roughly 40 nm wide. This observation is consistent with the high crystallinity of this material and can explain the higher hole mobility in OFETs prepared with this material, at least compared to **CA-5T-IID-5T-CA-b** and **CA-4T-IID-4T-CA-b**, which appeared to provide rather featureless (and possibly largely amorphous) films (Fig. 5c and e). At the same time, **CA-3T-IID-**

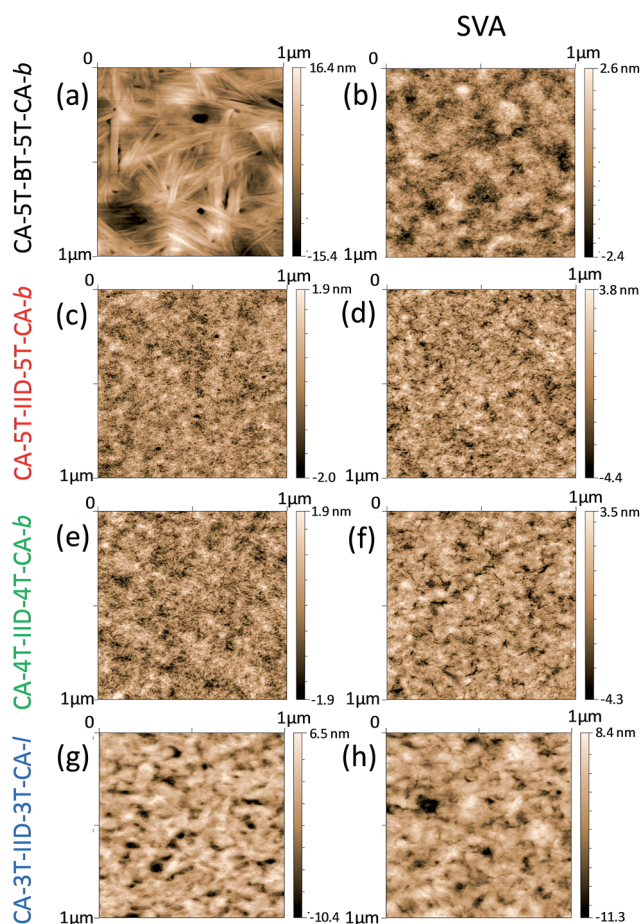


Fig. 5 AFM images (1 μm × 1 μm) of pure small molecule films before (a, c, e and g) and after (b, d, f and h) exposing the films to a vapour of dichloromethane (SVA).

Table 2 Device performance parameters for the BHJ organic solar cells based on the different small molecule:PC<sub>71</sub>BM blends<sup>a</sup>

Donor	SVA <sup>b</sup> (s)	$\mu$ (cm <sup>2</sup> V <sup>-1</sup> s <sup>-1</sup> )	V <sub>oc</sub> (V)	J <sub>sc</sub> (mA cm <sup>-2</sup> )	FF (%)	PCE <sup>c</sup> (%)	J <sub>EQE</sub> (mA cm <sup>-2</sup> )
<b>CA-5T-BT-5T-CA-b</b>		$1.44 \times 10^{-5}$	0.78	2.42	45	0.85 (0.84 ± 0.01)	2.62
<b>CA-5T-IID-5T-CA-b</b>	10	$6.70 \times 10^{-5}$	0.68	1.14	52	0.40 (0.33 ± 0.09)	1.32
<b>CA-5T-IID-5T-CA-b</b>		$3.75 \times 10^{-6}$	0.87	1.81	50	0.80 (0.74 ± 0.05)	1.96
<b>CA-5T-IID-5T-CA-b</b>	10	$3.44 \times 10^{-5}$	0.83	3.29	51	1.39 (1.10 ± 0.21)	3.29
<b>CA-4T-IID-4T-CA-b</b>		$4.26 \times 10^{-6}$	0.99	0.94	51	0.47 (0.45 ± 0.02)	0.94
<b>CA-4T-IID-4T-CA-b</b>	10	$1.86 \times 10^{-5}$	0.98	1.60	50	0.78 (0.70 ± 0.05)	1.61
<b>CA-3T-IID-3T-CA-I</b>		$4.20 \times 10^{-4}$	0.96	1.32	55	0.69 (0.65 ± 0.02)	1.46
<b>CA-3T-IID-3T-CA-I</b>	10	$3.66 \times 10^{-3}$	0.95	4.46	45	1.92 (1.60 ± 0.20)	4.33

<sup>a</sup> All processing from CHCl<sub>3</sub> (1 : 0.8 w/w ratio), no thermal annealing applied. <sup>b</sup> Solvent vapour annealing. <sup>c</sup> Best efficiencies. Averages over at least 4 devices in parentheses.

**3T-CA-I** tends to form thinner fibers, which cluster in aggregates of approximately  $1500 \text{ nm}^2$  (Fig. 5g). Comparing the hole mobilities of **CA-3T-IID-3T-CA-I** and **CA-5T-BT-5T-CA-b** suggests that the large fibrils of the latter are not as favourably aligned for planar hole transport as in the case of the linear molecule. After SVA, all hole mobilities increased, but the effect was most pronounced for the three IID-based molecules (Table 2). The surface morphologies of the thin films changed slightly into larger features upon solvent vapour treatment, with the exception of the BT-based small molecule, which lost its pronounced fibrillary structure (Fig. 5b). The obtained hole mobilities are comparable with those of other IID-based small molecules recently reported in the literature.<sup>32</sup>

### 3.3. Organic solar cells

The photovoltaic performances of the novel molecular semiconductors were evaluated by fabricating conventional BHJ organic solar cells in the configuration glass/ITO/PEDOT:PSS/small molecule:PC<sub>71</sub>BM/Ca/Al. Solar cell fabrication and characterization were performed in a glovebox under nitrogen atmosphere. After some optimization, chloroform was selected as the optimal processing solvent for the photoactive layers. For all small molecule blends, the best performance was obtained by spin-coating the donor:PC<sub>71</sub>BM blends in a 1 : 0.8 w/w ratio (Tables S1–S4†). Film thickness and SVA were systematically investigated for all the blends. The achieved solar cell performance parameters and representative current density–voltage (*J*–*V*) curves are shown in Table 2 and Fig. 6a, respectively. The best device efficiency for the branched BT-based molecule (**CA-5T-BT-5T-CA-b**) was obtained without SVA treatment ( $J_{\text{sc}} = 2.42 \text{ mA cm}^{-2}$ ,  $V_{\text{oc}} = 0.78 \text{ V}$ , FF = 45%; PCE = 0.85%). The annealed device shows a drop in open-circuit voltage ( $V_{\text{oc}}$ ) and short-circuit current density ( $J_{\text{sc}}$ ), despite the increased hole mobility observed for the pure donor compound upon SVA. In contrast, the analogous IID-based molecule (**CA-5T-IID-5T-CA-b**) exhibits a better performance after SVA ( $J_{\text{sc}} = 3.29 \text{ mA cm}^{-2}$ ,  $V_{\text{oc}} = 0.83 \text{ V}$ , FF = 51%; PCE = 1.39%), mainly due to a current increase. As expected based on

the electrochemical results, the removal of one hexylthiophene unit (**CA-4T-IID-4T-CA-b**) leads to an enhanced  $V_{\text{oc}}$ , which is unfortunately compensated by the very low  $J_{\text{sc}}$ . The best result was again obtained after SVA ( $J_{\text{sc}} = 1.60 \text{ mA cm}^{-2}$ ,  $V_{\text{oc}} = 0.98 \text{ V}$ , FF = 50%; PCE = 0.78%). The highest photovoltaic efficiency within the series was obtained with the linear IID-based small molecule **CA-3T-IID-3T-CA-I**. Also in this case, the device performance noticeably improved after SVA ( $J_{\text{sc}} = 4.46 \text{ mA cm}^{-2}$ ,  $V_{\text{oc}} = 0.95 \text{ V}$ , FF = 45%; PCE = 1.92%), despite the reduction in fill factor (FF).

The external quantum efficiencies of the organic solar cells before and after SVA were measured as well (Fig. 6b). The photocurrents obtained by integration of the EQE spectra are comparable to the  $J_{\text{sc}}$  values obtained from the *I*–*V* measurements (Table 2). Charge carriers are generated and collected over the full region between 300 and 750 nm for all small molecule blends. As mentioned above, the performances of the IID-based small molecule devices improve upon SVA.

The effect of SVA on the OPV device performance was further investigated by studying the surface morphology of the active layers by AFM (Fig. 7). From the *J*–*V* and EQE results, the efficiency of the solar cell based on **CA-5T-BT-5T-CA-b** decreased upon SVA due to a reduction in  $J_{\text{sc}}$ . From the AFM images it can be seen that the pristine active layer shows domains with a diameter of  $\sim 80 \text{ nm}$ . The size of the domains increases considerably (diameter above 200 nm) after SVA, unfavorable for effective charge separation. The opposite trend is observed for the IID-based small molecules, for which the device performances generally improved after SVA. The topography images of the active layers based on the **CA-5T-IID-5T-CA-b**:PC<sub>71</sub>BM and **CA-4T-IID-4T-CA-b**:PC<sub>71</sub>BM blends also show domains of  $\sim 100$ – $200 \text{ nm}$ . After SVA, the separate phases are less defined. The improved performances could be attributed to a more favorable charge separation provided by the new morphology. The pristine active layer constructed from the linear **CA-3T-IID-3T-CA-I** small molecule does not present well-defined aggregates. After SVA, the thin film became more homogeneous, uniform and flat, increasing the interfacial area

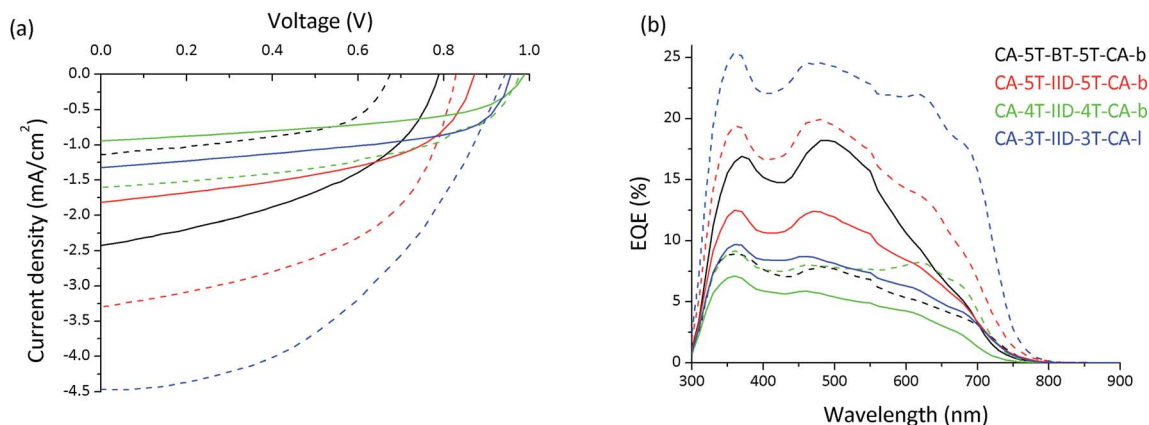


Fig. 6 (a) *J*–*V* characteristics and (b) EQE spectra of optimized BHJ organic solar cells made from **CA-5T-BT-5T-CA-b**:PC<sub>71</sub>BM (black), **CA-5T-IID-5T-CA-b**:PC<sub>71</sub>BM (red), **CA-4T-IID-4T-CA-b**:PC<sub>71</sub>BM (green), and **CA-3T-IID-3T-CA-I**:PC<sub>71</sub>BM (blue) before (solid lines) and after SVA (dashed lines).

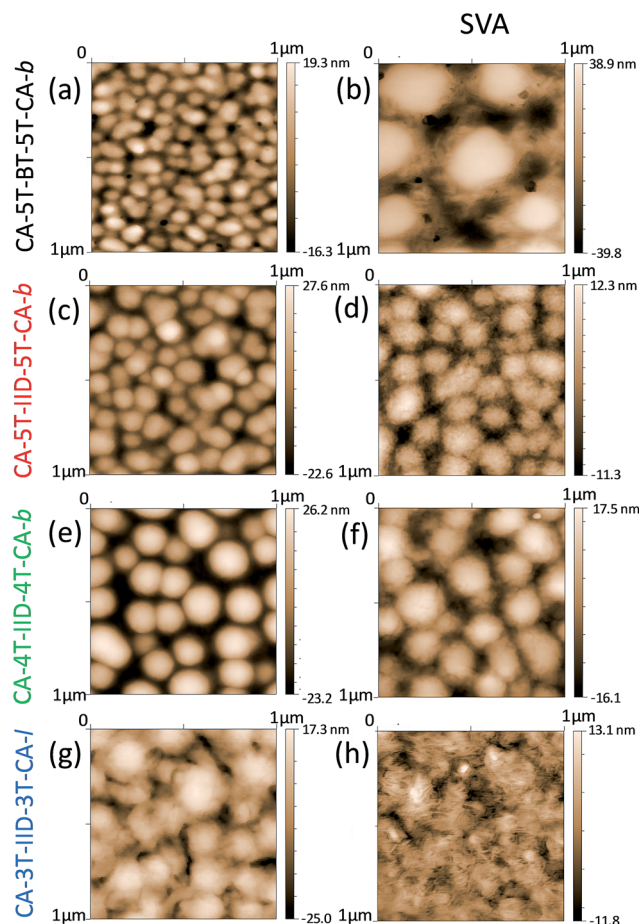


Fig. 7 AFM images ( $1 \mu\text{m} \times 1 \mu\text{m}$ ) for the BJJ OPV devices without (a, c, e and g) and with (b, d, f and h) exposure of the active layer to vapour of dichloromethane.

between the small molecule and PC<sub>71</sub>BM, in agreement with the enhanced  $J_{\text{sc}}$  and efficiency. Within the studied series, the CA-3T-IID-3T-CA-I clearly gives rise to the most desirable active layer morphology, although the lower FF upon SVA may be an indication that percolation to the collecting electrodes became more difficult after the post-treatment.<sup>57</sup>

## 4. Conclusions

In summary, a series of A<sub>2</sub>-D-A<sub>1</sub>-D-A<sub>2</sub> solution-processable small molecules have been synthesized to probe structure-property correlations for organic photovoltaic and transistor applications. Exchange of the central benzothiadiazole acceptor by an isoindigo moiety resulted in deeper HOMO-LUMO energy levels, enabling higher open-circuit voltages to be reached in bulk heterojunction organic solar cells. The linear architecture of the CA-3T-IID-3T-CA-I small molecule leads to a red-shifted absorption maximum, increased stacking behaviour, a higher (pure film) hole mobility ( $3.66 \times 10^{-3} \text{ cm}^2 \text{ V}^{-1} \text{ s}^{-1}$ ), and the most favourable active layer morphology, which allowed for the highest power conversion efficiency (1.9%). The other small molecule:PC<sub>71</sub>BM blends mainly suffer from low short-circuit currents that can be related to unfavourable active layer blend

morphologies, as evidenced by AFM. Our observations highlight the crucial role played by molecular structure/architecture and thin film morphology in the performance of organic solar cells and field-effect transistors,<sup>42,58</sup> and the possibility to exploit solvent vapour treatments towards an optimized transistor and bulk heterojunction solar cell active layer.

## Acknowledgements

This work was supported by the project ORGANEXT (EMR INT4-1.2-2009-04/054), selected in the frame of the operational program INTERREG IV-A Euregio Maas-Rijn. The European Commission and Walloon Region are acknowledged in the frame of this INTERREG project. We are also grateful for the support by the Science Policy Office of the Belgian Federal Government (BELSPO; IAP 7/05 – Functional Supramolecular Systems) and the National Funds for Scientific Research (F.R.S.-FNRS). The authors thank H. Penxten (UHasselt) for her valuable help with the CV and UV-vis measurements. C. D. is Research Director by F.R.S.-FNRS.

## References

- 1 H. C. Liao, C. C. Ho, C. Y. Chang, M. H. Jao, S. B. Darling and W. F. Su, *Mater. Today*, 2013, **16**, 326.
- 2 S. Lizin, S. van Passel, E. de Schepper, W. Maes, L. Lutsen, J. Manca and D. Vanderzande, *Energy Environ. Sci.*, 2013, **6**, 3136.
- 3 A. J. Heeger, *Adv. Mater.*, 2014, **26**, 10.
- 4 H. W. Choi, T. Zhou, M. Singh and G. E. Jabbour, *Nanoscale*, 2015, **7**, 3338.
- 5 H. Minemawari, T. Yamada, H. Matsui, J. Tsutsumi, S. Haas, R. Chiba, R. Kumai and T. Hasegawa, *Nature*, 2011, **475**, 364.
- 6 G. Giri, E. Verploegen, S. C. B. Mannsfeld, S. Atahan-Evrenk, D. H. Kim, S. Y. Lee, H. A. Becerril, A. Aspuru-Guzik, M. F. Toney and Z. Bao, *Nature*, 2011, **480**, 504.
- 7 H. Dong, X. Fu, J. Liu, Z. Wang and W. Hu, *Adv. Mater.*, 2013, **25**, 6158.
- 8 A. K. K. Kyaw, D. H. Wang, D. Wynands, J. Zhang, T.-Q. Nguyen, G. C. Bazan and A. J. Heeger, *Nano Lett.*, 2013, **13**, 3796.
- 9 Y. Liu, Y. Yang, C.-C. Chen, Q. Chen, L. Dou, Z. Hong, G. Li and Y. Yang, *Adv. Mater.*, 2013, **25**, 4657.
- 10 D. Liu, M. Xiao, Z. Du, Y. Yan, L. Han, V. A. L. Roy, M. Sun, W. Zhu, C. S. Lee and R. Yang, *J. Mater. Chem. C*, 2014, **2**, 7523.
- 11 Q. Zhang, B. Kan, F. Liu, G. Long, X. Wan, X. Chen, Y. Zou, W. Ni, H. Zang, M. Li, Z. Hu, F. Huang, Y. Cao, Z. Liang, M. Zang, T. P. Russell and Y. Chen, *Nat. Photonics*, 2015, **9**, 35.
- 12 K. Sun, Z. Xiao, S. Lu, W. Zajaczkowski, W. Pisula, E. Hanssen, J. M. White, R. M. Williamson, J. Subbiah, J. Ouyang, A. B. Holmes, W. W. H. Wong and D. J. Jones, *Nat. Commun.*, 2015, **6**, 6013.
- 13 K. Gao, L. Li, T. Lai, L. Xiao, Y. Huang, F. Huang, J. Peng, Y. Cao, F. Liu, T. P. Russell, R. A. J. Janssen and X. Peng, *J. Am. Chem. Soc.*, 2015, **137**, 7282.

- 14 B. Kan, M. Li, Q. Zhang, F. Liu, X. Wan, Y. Wang, W. Ni, G. Long, X. Yang, H. Feng, Y. Zuo, M. Zhang, F. Huang, Y. Cao, T. P. Russell and Y. Chen, *J. Am. Chem. Soc.*, 2015, **137**, 3886.
- 15 Y. Lin, Y. Li and X. Zhan, *Chem. Soc. Rev.*, 2012, **41**, 4245.
- 16 Y. Chen, X. Wan and G. Long, *Acc. Chem. Res.*, 2013, **46**, 2645.
- 17 D. Bagnis, L. Beverina, H. Huang, F. Silvestri, Y. Yao, H. Yan, G. A. Pagani, T. J. Marks and A. Facchetti, *J. Am. Chem. Soc.*, 2010, **132**, 4074.
- 18 M. F. G. Klein, F. Pasker, H. Wettach, I. Gadaczek, T. Bredow, P. Zilkens, P. Vöhringer, U. Lemmer, S. Höger and A. Colsmann, *J. Phys. Chem. C*, 2012, **116**, 16358.
- 19 Y. Liu, X. Wan, F. Wang, J. Zhou, G. Long, J. Tian, J. You, Y. Yang and Y. Chen, *Adv. Energy Mater.*, 2011, **1**, 771.
- 20 H.-F. Feng, W.-F. Fu, L. Li, Q.-C. Yu, H. Lu, J.-H. Wan, M.-M. Shi, H.-Z. Chen, Z. Tan and Y. Li, *Org. Electron.*, 2014, **15**, 2575.
- 21 Y. Chen, Y. Yan, Z. Du, X. Bao, Q. Liu, V. A. L. Roy, M. Sun, R. Yang and C. S. Lee, *J. Mater. Chem. C*, 2014, **2**, 3921.
- 22 R. Stalder, J. Mei, K. R. Graham, L. A. Estrada and J. R. Reynolds, *Chem. Mater.*, 2014, **26**, 664.
- 23 T. Maugard, E. Enaud, P. Choisy and M. D. Legoy, *Phytochemistry*, 2001, **58**, 897.
- 24 G. Zhang, Y. Fu, Z. Xie and Q. Zhang, *Macromolecules*, 2011, **44**, 1414.
- 25 E. Wang, Z. Ma, Z. Zhang, P. Henriksson, O. Inganäs, F. Zhang and M. R. Andersson, *Chem. Commun.*, 2011, **47**, 4908.
- 26 Z. Ma, E. Wang, M. E. Jarvid, P. Henriksson, O. Inganäs, F. Zhang and M. R. Andersson, *J. Mater. Chem.*, 2012, **22**, 2306.
- 27 E. Wang, W. Mammo and M. R. Andersson, *Adv. Mater.*, 2014, **26**, 1801.
- 28 J. Mei, K. R. Graham, R. Stalder and J. R. Reynolds, *Org. Lett.*, 2010, **12**, 660.
- 29 Z. Ma, W. Sun, S. Himmelberger, K. Vandewal, Z. Tang, J. Bergqvist, A. Salleo, J. W. Andreasen, O. Inganäs, M. R. Andersson, C. Müller, F. Zhang and E. Wang, *Energy Environ. Sci.*, 2014, **7**, 361.
- 30 N. M. Randell, A. F. Douglas and T. L. Kelly, *J. Mater. Chem. A*, 2014, **2**, 1085.
- 31 Y. Ren, A. K. Hailey, A. M. Hiszpanski and Y. Loo, *Chem. Mater.*, 2014, **26**, 6570.
- 32 Y. J. Park, J. H. Seo, W. Elsayy, B. Walker, S. Cho and J.-S. Lee, *J. Mater. Chem. C*, 2015, **3**, 5951.
- 33 H. Kang, S. An, B. Walker, S. Song, T. Kim, J. Y. Kim and C. Yang, *J. Mater. Chem. A*, 2015, **3**, 9899.
- 34 J. Areephong, R. R. San Juan, A.-J. Payne and G. C. Welch, *New J. Chem.*, 2015, **39**, 5075.
- 35 P. Zhou, D. Dang, Q. Wang, X. Duan, M. Xiao, Q. Tao, H. Tan, R. Yang and W. Zhu, *J. Mater. Chem. A*, 2015, **3**, 13568.
- 36 M. Tomassetti, F. Ouhib, A. Wislez, A.-S. Duwez, H. Penxten, W. Dierckx, I. Cardinaletti, R. A. A. Bovee, G. W. P. van Pruissen, C. Jérôme, J. Manca, W. Maes and C. Detrembleur, *Polym. Chem.*, 2015, **6**, 6040.
- 37 J.-Y. Pan, L.-J. Zuo, X.-L. Hu, W.-F. Fu, M.-R. Chen, L. Fu, X. Gu, H.-Q. Shi, M.-M. Shi, H.-Y. Li and H.-Z. Chen, *ACS Appl. Mater. Interfaces*, 2013, **5**, 972.
- 38 N. Prachumrak, S. Pojanasopa, S. Namuangruk, T. Kaewin, S. Jungsuttiwong, T. Sudyoasuk and V. Promarak, *ACS Appl. Mater. Interfaces*, 2013, **5**, 8694.
- 39 P. B. Pati, S. P. Senanayak, K. S. Narayan and S. S. Zade, *ACS Appl. Mater. Interfaces*, 2013, **5**, 12460.
- 40 J. Min, Y. N. Luponosov, A. N. Solodukhin, N. Kaush-Busies, S. A. Ponomarenko, T. Ameri and C. J. Brabec, *J. Mater. Chem. C*, 2014, **2**, 7614.
- 41 S. Paek, H. Choi, J. Sim, K. Song, J. K. Lee and J. Ko, *J. Phys. Chem. C*, 2014, **118**, 27193.
- 42 F. Ouhib, M. Tomassetti, W. Dierckx, P. Verstappen, A. Wislez, A. Duwez, V. Lemaure, R. Lazzaroni, J. Manca, W. Maes, C. Jérôme and C. Detrembleur, *Org. Electron.*, 2015, **20**, 76.
- 43 L. Meng, F. Wu, H. Liu, B. Zhao, J. Zhang, J. Zhong, Y. Pei, H. Chen and S. Tan, *RSC Adv.*, 2015, **5**, 14540.
- 44 H. Bai, Y. Wang, P. Cheng, Y. Li, D. Zhu and X. Zhan, *ACS Appl. Mater. Interfaces*, 2014, **6**, 8426.
- 45 Z. Li, G. He, X. Wan, Y. Liu, J. Zhou, G. Long, Y. Zuo, M. Zhang and Y. Chen, *Adv. Energy Mater.*, 2012, **2**, 74.
- 46 G. He, Z. Li, X. Wan, Y. Liu, J. Zhou, G. Long, M. Zhang and Y. Chen, *J. Mater. Chem.*, 2012, **22**, 9173.
- 47 J. Zhou, X. Wan, Y. Liu, Z. Li, G. He, G. Long, W. Ni, C. Li, X. Su and Y. Chen, *J. Am. Chem. Soc.*, 2012, **134**, 16345.
- 48 G. He, X. Wan, Z. Li, Q. Zhang, G. Long, Y. Liu, Y. Hou, M. Zhang and Y. Chen, *J. Mater. Chem. C*, 2014, **2**, 1337.
- 49 M. M. M. Raposo, A. M. C. Fonseca and G. Kirsch, *Tetrahedron*, 2004, **60**, 4071.
- 50 S. Telitel, F. Ouhib, J. Fouassier, C. Jérôme, C. Detrembleur and J. Lalevée, *Macromol. Chem. Phys.*, 2014, **215**, 1514.
- 51 A. J. Bard and L. R. Faulkner, *Electrochemical methods: fundamentals and applications*, Wiley, 2nd edn, 2001.
- 52 S. Trasatti, *Pure Appl. Chem.*, 1986, **58**, 955.
- 53 F. Würthner, T. E. Kaiser and C. R. Saha-Möller, *Angew. Chem., Int. Ed.*, 2011, **50**, 3376.
- 54 M. C. Scharber, D. Mühlbacher, M. Koppe, P. Denk, C. Waldauf, A. J. Heeger and C. J. Brabec, *Adv. Mater.*, 2006, **18**, 789.
- 55 H. Zhou, L. Yang and W. You, *Macromolecules*, 2012, **45**, 607.
- 56 W. Zhuang, M. Bolognesi, M. Seri, P. Henriksson, D. Gedefaw, R. Kroon, M. Jarvid, A. Lundin, E. Wang, M. Muccini and M. R. Andersson, *Macromolecules*, 2013, **46**, 8488.
- 57 B. Ray and M. A. Alam, *Sol. Energy Mater. Sol. Cells*, 2012, **99**, 204.
- 58 I. Cardinaletti, J. Kesters, S. Bertho, B. Conings, F. Piersimoni, J. D'Haen, L. Lutsen, M. Nesladek, B. van Mele, G. van Assche, K. Vandewal, A. Salleo, D. Vanderzande, W. Maes and J. V. Manca, *J. Photonics Energy*, 2014, **4**, 040997.